

Longitudinal versus transverse spheroidal vibrational modes of an elastic sphere

Lucien Saviot¹ and Daniel B. Murray²

¹*Laboratoire de Recherche sur la Réactivité des Solides, UMR 5613 CNRS - Université de Bourgogne
9 avenue A. Savary, BP 47870 - 21078 Dijon - France**

²*Department of Physics and Astronomy, Okanagan University College,
3333 University Way, Kelowna, British Columbia, Canada V1V 1V7†*

(Dated: February 19, 2019)

Analysis of the spheroidal modes of vibration of a free elastic sphere show that they can be qualitatively grouped into two categories: primarily longitudinal and primarily transverse. This is not a sharp distinction. However, there is a relatively stark contrast between the two kinds of modes. Primarily transverse modes have a small divergence and have frequencies that are almost functionally independent of the longitudinal speed of sound. Analysis of inelastic light scattering intensity from confined acoustic phonons in nanoparticles requires an understanding of this qualitative distinction between different spheroidal modes. In addition, some common misconceptions about spheroidal modes are corrected.

PACS numbers: 62.20.-x,43.20.Ks,62.25.+g

I. INTRODUCTION

With the explosion of interest in the optical properties of nanoparticles, the classic elastic mechanical problem of the vibrational modes of a free continuum sphere has found a new context for application. The problem was formally and numerically solved back in 1882.¹ Nanoparticles, *i.e.* spherical clusters of atoms ranging in diameter from 1 nm to 100 nm, have sufficiently few atoms that the continuum approximation can be questioned. Even so, it is acceptable to ignore the effects of the discrete crystal lattice for the few vibrational modes with lowest frequency.

Inelastic light scattering of a continuous laser beam shining on the nanoparticle permits detection of the mechanical vibrations since the changing size and shape of the nanoparticle modulates the polarizability of the nanoparticle, so that the monochromatic incident light turns into scattered light with sidebands shifted up and down by the frequency of the vibrations. This can be seen using experimental setups of the Raman and Brillouin type.

For theoretical convenience the material is assumed to be homogeneous, isotropic and linear. The outer surface of the sphere is free from externally imposed stresses and this situation will be referred to as the “free sphere model” (FSM). The original paper by Lamb¹ classified the FSM modes of vibration into two classes, now called “torsional” (TOR) and “spheroidal” (SPH). The distinctive feature of torsional modes is that the material density does not vary. In other words, the divergence of the displacement field is zero. Furthermore, the spherical symmetry permits classification of the modes by angular momentum number $\ell \geq 0$. (However, later on we will show that there is value in considering ℓ to be a continuous variable.) There is no dependence of the frequency on the z angular momentum m . Beyond this, the modes are indexed by $n \geq 0$. It is convenient to let p denote either SPH or TOR, to indicate individual modes by (p, ℓ, n)

and their frequencies by $\omega_{p\ell n}$.

What we explore in this paper is an additional classification of the SPH modes beyond that employed since Lamb. In particular, SPH modes can be classified (albeit approximately and subjectively) as either being primarily longitudinal (SPH_L) or primarily transverse (SPH_T) in nature. The specific meaning of this will be explained further on. This is not a sharp division, and actual modes fall somewhere in between the two ideals. However, the contrast is sufficiently sharp that this new distinction among SPH FSM modes as SPH_L or SPH_T is a very important tool.

In a recent theoretical paper, G. Bachelier and A. Mlayah² predicted that $(SPH, \ell = 2, n)$ modes with differing values of n contribute to the Raman spectrum in a highly non-uniform way. In this paper we will show that this can be explained using the previously mentioned distinction between SPH modes. They pointed out that there are two separate mechanisms that couple $(SPH, \ell = 2)$ acoustic vibrations to the surface plasmon resonance and in turn lead to Raman scattering. First, change of the particle shape and second, modulation of the density leading to change of optical properties through the deformation potential.

Section II reprises the formalism necessary for the FSM solution. In Section III, we show explicitly what we mean by SPH_L and SPH_T. In Section IV, we illustrate the natural appearance of SPH_L and SPH_T modes in the high frequency limit. Section V discusses these results and their connection with inelastic light scattering experiments.

II. THE FREE SPHERE MODEL

Vibrational modes of a free linear elastic continuum homogeneous isotropic sphere were found by Lamb in 1882.¹

For a mode with angular frequency ω , the displace-

ment of material point \vec{r} from its equilibrium position is $\vec{u}(\vec{r})\cos(\omega t)$. For a $m = 0$ TOR mode, $\vec{u} = A \nabla \times (\vec{r} j_\ell(k_T r) P_\ell(\cos\theta))$, where j_ℓ are spherical Bessel functions of the first kind and P_ℓ are Legendre polynomials. For a $m = 0$ SPH mode, $\vec{u} = \vec{u}_L + \vec{u}_T$ where

$$\vec{u}_L(r, \theta) = B \nabla j_\ell(k_L r) P_\ell(\cos\theta) \quad (1)$$

and

$$\vec{u}_T(r, \theta) = C \nabla \times \nabla \times (\vec{r} j_\ell(k_T r) P_\ell(\cos\theta)) \quad (2)$$

where A , B and C are real coefficients, $v_L k_L = v_T k_T = \omega$, and v_T and v_L are the transverse and longitudinal speeds of sound.

Modes with z angular momentum $m \neq 0$ have a different functional form.

R is the nanoparticle radius. If σ_{ij} is the stress tensor, the boundary conditions at $r = R$ are $\sigma_{rr} = \sigma_{r\theta} = 0$. It is convenient to introduce dimensionless frequencies $\eta = k_T R$ and $\xi = k_L R$. Following Eringen,³ application of these boundary conditions determines the allowed SPH vibrational frequencies as zeroes of a 2×2 determinant for $\ell > 0$.

$$\Delta_\ell = \begin{vmatrix} T_{11} & T_{13} \\ T_{41} & T_{43} \end{vmatrix} \quad (3)$$

where

$$\begin{aligned} T_{11} &= \left(\ell^2 - \ell - \frac{\eta^2}{2} \right) j_\ell(\xi) + 2\xi j_{\ell+1}(\xi) \\ T_{13} &= \ell(\ell+1) \{ (\ell-1)j_\ell(\eta) - \eta j_{\ell+1}(\eta) \} \\ T_{41} &= (\ell-1)j_\ell(\xi) - \xi j_{\ell+1}(\xi) \\ T_{43} &= \left(\ell^2 - 1 - \frac{\eta^2}{2} \right) j_\ell(\eta) + \eta j_{\ell+1}(\eta) \end{aligned}$$

For $\ell = 0$, the allowed vibrational frequencies are the zeroes of T_{11} .

Noting that the displacement fields are real-valued, it is appropriate to use the following inner product between two displacement fields u_A and u_B :⁴

$$(u_A | u_B) = \frac{\int_{r < R} \vec{u}_A(\vec{r}) \cdot \vec{u}_B(\vec{r}) \rho d^3 r}{\int_{r < R} \rho d^3 r} \quad (4)$$

A normalization condition (such as $(u | u) = 1$) would typically determine the final values of B and C . But the details of the condition do not affect the results reported here. The displacement field $\vec{u}(\vec{r})$ for some selected modes are depicted in Fig. 1.

III. SPHEROIDAL MODE LONGITUDINALITY

Isotropic elastic materials differ in their Poisson ratio, ν , which is related to $x = v_T/v_L$ through $x = \sqrt{(1-2\nu)/(2-2\nu)}$. Figure 2 shows how the dimensionless frequency, η , of the SPH $\ell = 2$ FSM modes varies

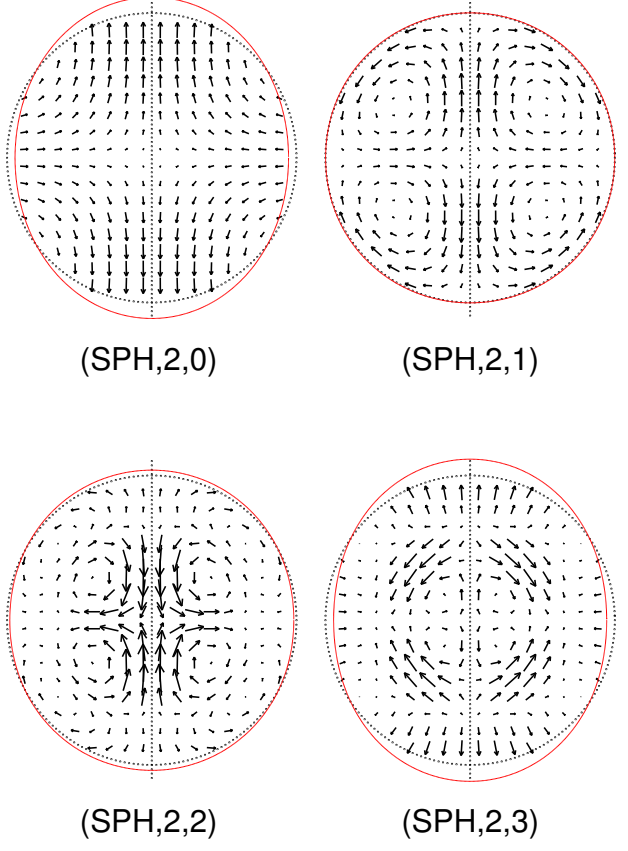


FIG. 1: Displacement fields $\vec{u}(\vec{r})$ of selected SPH $\ell=2$ modes. As explained in the text, the first three are primarily transverse (i.e. SPH_T). $(\text{SPH},2,3)$ is primarily longitudinal (i.e. SPH_L). The equilibrium surface of the nanoparticle and the z -axis are shown as dotted lines. The solid (red online) line shows the distorted surface. Note that the $(\text{SPH},2,1)$ mode does not change the nanoparticle shape.

with v_T/v_L . It is quite apparent that some modes keep the same η as v_T/v_L is varied. However, other modes change frequency as v_T/v_L changes. There are transition points where a given mode changes from being constant to varying with v_T/v_L .

This pattern visible in Fig. 2 motivates the search for a numerical criterion to permit this contrast among modes to be quantified. We adopt the starting point that in some sense some modes are more transverse in nature (SPH_T) while others are more longitudinal (SPH_L). We then coin the term “longitudinality”, denoted by L , for a quantity that varies on a scale from 0 to 1 with 0 being purely transverse and 1 being purely longitudinal. There is no single obvious way of doing this. Rather, we have evaluated a number of quantities as candidates for the best measure of longitudinality, of which we present four which work well. These will be denoted $L1$, $L2$, $L3$, and $L4$.

Consider a particular SPH mode with indices ℓ and n .

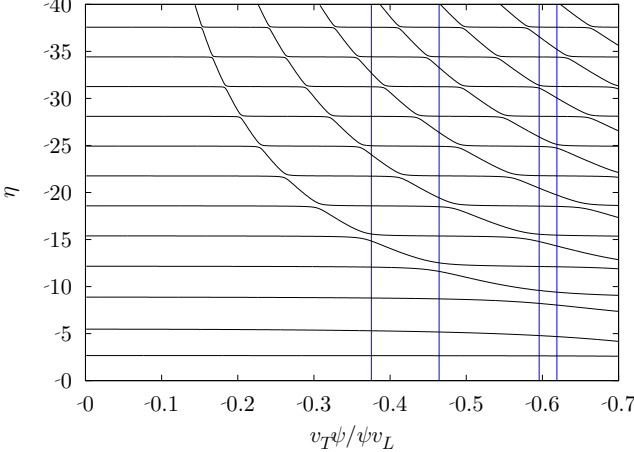


FIG. 2: Dimensionless mode frequency η as a function of v_T/v_L for (SPH, $\ell = 2$) modes. Vertical lines mark v_T/v_L for Au, Ag, Si and Ge from left to right.

Its frequency is $\omega(v_L, v_T)$. Define $L1$ by

$$L1 = \frac{v_L}{\omega} \frac{\partial \omega}{\partial v_L} = -\frac{x}{\eta} \frac{d\eta}{dx} = 1 - \frac{v_T}{\omega} \frac{\partial \omega}{\partial v_T} \quad (5)$$

Noting that $\vec{u}(\vec{r}) = \vec{u}_T(\vec{r}) + \vec{u}_L(\vec{r})$, we define $L2$ as $(u_L|u_L)/(u|u)$, and $L3$ as $1 - ((u_T|u_T)/(u|u))$. But note also that $(u_L|u_L) + (u_T|u_T) \neq (u|u)$ since $(u_L|u_T) \neq 0$.

Given a fixed value of v_T/v_L and n , η may be considered to be a continuous function of ℓ , as in Fig. 3. In terms of this $\eta(\ell)$, define

$$L4 = \frac{v_T}{v_L - v_T} \left(\frac{2}{\pi} \frac{d\eta}{d\ell} - 1 \right) \quad (6)$$

Let $\langle \dots \rangle_V$ and $\langle \dots \rangle_S$ denote averages over the nanoparticle volume and surface, respectively. In particular, $(u|u) = \langle u_r^2 + u_\theta^2 + u_\phi^2 \rangle_V$. Some other measures of interest are as follows: URV = $\langle u_r^2 \rangle_V / (u|u)$, URS = $\langle u_r^2 \rangle_S / (u|u)$, UTS = $\langle u_\theta^2 + u_\phi^2 \rangle_S / (u|u)$, and U2S = URS + UTS.

Note that all of these quantities are defined in such a way as to be independent of m .

Except at low η , Fig. 4 shows that $L1$ and $L2$ are in close agreement. $L3$ and $L4$ are not plotted, but also agree closely except at low η . Generally, a given mode either has all of $L1$, $L2$, $L3$, and $L4$ low, or else all high. It is thus possible to classify modes as SPH_L or SPH_T . Rarely, there are cases where the values of $L1$, $L2$, $L3$, and $L4$ are in the intermediate range, such as in Fig. 4 for $\ell = 3$ for the two modes near $\eta = 13$. Such modes which are neither clearly SPH_L nor SPH_T always occur in pairs. The reason for this is explained in Section IV.

Table I provides additional information about the modes. The dimensionless frequency η is provided for convenience, as is the ratio of coefficients B and C .

In principle, C/B could be expected to provide useful information about whether a mode is SPH_L or SPH_T .

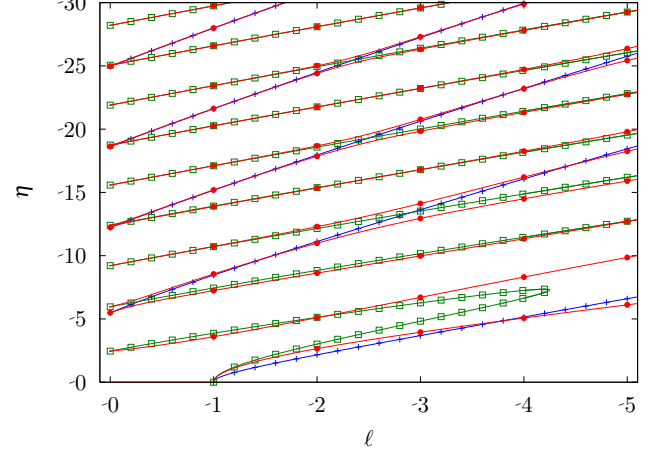


FIG. 3: Variation of the SPH mode frequency with ℓ for a material with $v_T/v_L = 0.5$. Full circles are exact FSM frequencies and are connected with curves calculated for non-integer ℓ (red online). Lines with crosses are roots of T_{11} (blue online) which approximate SPH_L modes. Lines with empty squares are roots of T_{43} (green online) which approximate SPH_T modes.

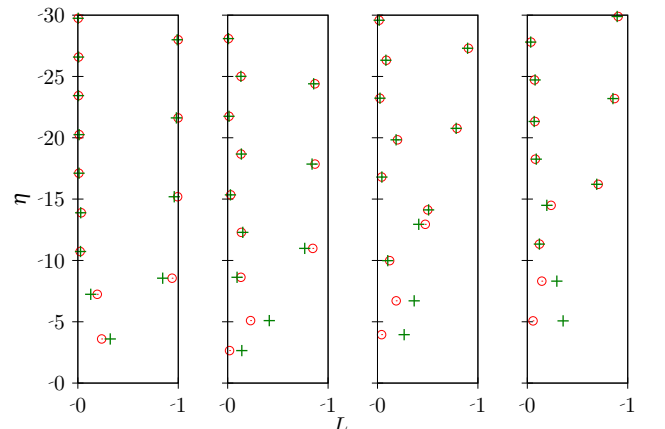


FIG. 4: Dimensionless mode frequency η as a function of longitudinality measures $L1$ (circles) and $L2$ (crosses) for SPH modes of a material with $v_T/v_L = 0.5$. $\ell = 1 \dots 4$ from left to right. SPH_T modes have $L1$ and $L2$ near zero, while for SPH_L modes they are close to 1.

In the extreme case that $C = 0$, the mode is evidently SPH_L , and likewise when $B = 0$ the mode is SPH_T . But the C/B values do not exhibit an informative pattern.

There is a strong contrast in the values of URS for different modes. However, it does not correlate to whether the mode is SPH_L or SPH_T except at high enough η . URS is an interesting quantity because it is the one we have to monitor for the surface deformation mechanism except for $\ell = 0$ modes.

Group theoretical arguments⁵ show that only SPH modes with $\ell=0$ and $\ell=2$ are Raman active. This assumes that the nanoparticle is perfectly spherical in

TABLE I: Other features of SPH modes for a material with $v_T/v_L = 0.5$.

ℓ	n	η	C/B	URV	URS	UTS	U2S	Class	n_L	n_T
0	0	5.49	0.00	1.00	0.91	0.00	0.91	SPH_L	0	
0	1	12.23	0.00	1.00	0.71	0.00	0.71	SPH_L	1	
0	2	18.63	0.00	1.00	0.68	0.00	0.68	SPH_L	2	
1	0	3.60	-0.99	0.37	0.05	1.26	1.31	SPH_T		0
1	1	7.24	1.65	0.43	0.14	0.66	0.81	SPH_T		1
1	2	8.55	-0.29	0.43	0.70	0.03	0.72	SPH_L	0	
1	3	10.73	4.37	0.21	0.00	0.69	0.69	SPH_T		2
1	4	13.89	-3.93	0.14	0.02	0.68	0.69	SPH_T		3
2	0	2.65	-0.44	0.59	0.66	0.20	0.86	SPH_T		0
2	1	5.10	-0.38	0.26	0.00	1.78	1.78	SPH_T		1
2	2	8.63	1.09	0.50	0.08	0.85	0.92	SPH_T		2
2	3	10.99	-0.22	0.35	0.71	0.04	0.75	SPH_L	0	
2	4	12.29	0.96	0.34	0.07	0.64	0.71	SPH_T		3
3	0	3.95	-0.17	0.74	0.89	0.03	0.91	SPH_T		0
3	1	6.71	-0.21	0.22	0.04	1.91	1.95	SPH_T		1
3	2	9.98	0.70	0.53	0.04	1.05	1.09	SPH_T		2
3	3	12.95	-0.33	0.35	0.43	0.41	0.84	mix	0	3
3	4	14.12	0.27	0.37	0.39	0.29	0.68	mix	0	3
4	0	5.07	-0.08	0.81	1.05	0.00	1.05	SPH_T		0
4	1	8.31	-0.15	0.23	0.14	1.78	1.92	SPH_T		1
4	2	11.33	0.46	0.54	0.01	1.25	1.27	SPH_T		2
4	3	14.49	-0.41	0.41	0.21	0.75	0.95	SPH_T		3
4	4	16.21	0.14	0.35	0.65	0.03	0.68	SPH_L	0	

shape and spherically symmetric in all of its properties. The basic nature of the $\ell = 0$ modes is much more clear because of their simplicity and symmetry. Consequently, the modes $(\text{SPH}, \ell = 2, n)$ are of primary interest when trying to understand Raman intensities.

From the value of $L2 \simeq 0.14$ in Tab. I, the displacement of $(\text{SPH}, 2, 0)$ is mostly due to the u_T term and not the u_L term. Its squared displacement due to the u_L term alone is just 14% of the total. The u_T term has zero divergence. Therefore, $(\text{SPH}, 2, 0)$ doesn't have much divergence. So the effect of changing density on the dielectric constant through the deformation potential may not be significant to the overall Raman intensity.

On the other hand, based on its URS of $\simeq 0.66$ and UTS of $\simeq 0.20$, the surface displacement of $(\text{SPH}, 2, 0)$ is strongly along r and only weakly along θ as Fig. 1 illustrates. Note that, r surface displacement changes the nanoparticle shape, while θ displacement does not.

The $(\text{SPH}, 2, 1)$ mode differs from $(\text{SPH}, 2, 0)$ in several ways. From the $L1$ value of 0.2281 in Fig. 4, we can see that the frequency of $(\text{SPH}, 2, 1)$ depends more on v_L . Also, $L2 \simeq 0.416$ in Fig. 4 shows that $(\text{SPH}, 2, 1)$ has more of a u_L component, even if it is still weaker than the u_T part. But this means that $(\text{SPH}, 2, 1)$ can have much more divergence than $(\text{SPH}, 2, 0)$. So the deformation potential mechanism can modulate the dielectric constant. But it

is very interesting to notice from the URS value of $\simeq 0.00$ in Tab. I (more precisely, 0.0003) that $(\text{SPH}, 2, 1)$ causes negligible radial movement of the surface. So $(\text{SPH}, 2, 1)$ barely changes the shape of the nanoparticle, as Fig. 1 shows.

$(\text{SPH}, 2, 3)$ has strong v_L dependence ($L1 \simeq 0.8475$) in Fig. 4 as well as a strong u_L component ($L2 \simeq 0.766$). So it is clear that it is SPH_L . Its surface displacement is mostly along r and not θ from its URS value of 0.71 and URT $\simeq 0.04$. So $(\text{SPH}, 2, 3)$ will strongly affect the shape of the nanoparticle surface, as shown in Fig. 1.

u_L and u_T take on simpler forms as η becomes larger. For large η , the u_L term has primarily radial displacement, while the u_T term corresponds to displacement in the θ direction.

For the lowest modes, the situation is qualitatively different. Consider $(\text{SPH}, 2, 0)$ with $v_T/v_L = 0.5$. Suppose to simplify this discussion we normalize the displacement field so that $(u|u) = 1$. Then $(u_L|u_L) \simeq 0.14$. However, $(u_T|u_T) \simeq 1.85$. So L3 for $(\text{SPH}, 2, 0)$ is actually $\simeq -0.85$, making it "ultra transverse" by that measure. It seems quite odd that the u_T term alone has a magnitude much greater than that of the overall motion. The resolution of this puzzle is that u_L and u_T are not mutually orthogonal with respect to the inner product of Eq. 4. In fact, $(u_T|u_L) \simeq -0.50$. According to the usual vector relation, $\vec{a} \cdot \vec{b} = \|\vec{a}\| \|\vec{b}\| \cos\theta_{ab}$, the "angle" between u_L and u_T is $\simeq 165$ degrees for the $(\text{SPH}, 2, 0)$ mode. This angle is nearly unchanged as v_T/v_L varies. Thus, u_L and u_T are nearly antiparallel vectors in the function space of vector fields within the nanoparticle interior. It can be said, then, that the functional forms of u_L and u_T are actually relatively similar. This is a bit of a surprise since one is curl-free while the other is divergence free. This angle between u_L and u_T rapidly approaches 90 degrees as η increases (*i.e.* for modes with higher n).

As Fig. 2 shows, the starkness of the contrast between SPH_L and SPH_T modes is at its best when v_T/v_L is lower. For materials with high v_T/v_L such as Si and Ge, FSM modes tend more to be mixtures of SPH_L and SPH_T , especially at low η . But the concept of longitudinality is quite applicable to materials such as Au and Ag.

IV. HIGH FREQUENCY MODE CLASSIFICATION

The reason for the dichotomy of SPH modes as SPH_T and SPH_L can be simply explained in the high frequency limit. Consider Δ_ℓ , the 2×2 determinant in Eq. 3, and its four matrix elements. Note that $\xi/\eta = v_T/v_L$. So at high frequency, both η and ξ are large. In that case, T_{11} and T_{43} will be much larger than T_{13} and T_{41} because of their terms including factors of η^2 . Consequently, Δ_ℓ is very well approximated by $T_{11}T_{43}$. Since normal modes correspond to zeroes of Δ_ℓ , it is clear that there will be two sets of modes: those which are approximately zeroes

of T_{11} and T_{43} respectively. The first group are SPH_L and the second group are SPH_T .

The roots of T_{11} and T_{43} are plotted versus ℓ in Fig. 3 with lines with crosses for SPH_L modes and lines with empty squares for SPH_T modes. The lines with full circles are the exact FSM mode frequencies.

There are three kinds of situations where we don't expect this approximation to be valid: (1) for low η (2) when it is not true that $\eta \gg \ell$ and (3) where longitudinal (T_{11}) and transverse (T_{43}) modes for a given ℓ are close – *i.e.* when the associated curves cross. Except in the previously mentioned places, the agreement between FSM and our approximation is quite good. The low η situation corresponds specifically to the similar prefactors of j_ℓ for T_{11} and T_{43} not being large. It is apparent that T_{11} and T_{43} can only be useful as estimators of SPH_L and SPH_T mode frequencies when $\eta \gg \ell$. This is confirmed from inspection of the lower right portion of Fig. 3.

For large x , $j_\ell(x) \simeq \sin(x - \ell\frac{\pi}{2})/x$. Therefore, for large ξ and η , the roots of T_{11} can be approximated by $\xi \simeq \ell\frac{\pi}{2} + (1+n_L)\pi$ and the roots of T_{43} by $\eta \simeq \ell\frac{\pi}{2} + n_T\pi$ where $n_L \geq 0$ and $n_T \geq 0$ are integers. These lead to remarkably compact approximate expressions for SPH_L and SPH_T FSM frequencies in Hertz, respectively:

$$f \simeq \frac{v_L}{d} \left(\frac{\ell}{2} + n_L + 1 \right) \quad (7)$$

$$f \simeq \frac{v_T}{d} \left(\frac{\ell}{2} + n_T \right) \quad (8)$$

where $d = 2R$. These expressions are very suggestive of the formula for acoustic standing waves in a one dimensional system of length d . Table I shows the value of either n_L or n_T for each mode.

The behaviour observed in Fig. 2 becomes simple to explain. To a good approximation, SPH FSM modes are either SPH_L or SPH_T . This approximation is considered here to be good because it gives the right number of vibrational modes and it predicts their frequency with a reasonable accuracy.

“Anti-crossing” is observed in Fig. 2 each time the variation of the frequency of a SPH_L mode crosses the one of a SPH_T mode. In Fig. 2 there are two kinds of curves: horizontal lines for SPH_T modes and descending curves for SPH_L ones. Then, each time these curves come together, an anti-crossing pattern appears for the FSM solutions. In Fig. 3, FSM frequencies η are plotted versus ℓ for a sphere made of a material which has $v_T/v_L = 0.5$. Because the SPH_L and SPH_T approximation curves are plotted, the anti-crossing patterns are clearly revealed. The continuation of Bessel functions to non-integer ℓ permits relationships among modes for different integer ℓ to be clearly seen. This is preferable to the common practice of joining modes on such a graph with hand-drawn straight lines.

V. DISCUSSION:

Normal elastic waves in a solid have a longitudinal acoustic (LA) branch and two transverse acoustic (TA) branches. However, for FSM it seemed there are just two kinds: SPH and TOR . By classifying SPH modes into two kinds (*i.e.* SPH_L and SPH_T), there are now three categories of modes, as we would expect.

We plot in Fig. 5 the mean squared radial surface displacement (URS) at the surface of a 5 nm diameter silver nanoparticle for all $\text{SPH } \ell = 2$ modes. The magnitude of URS is in good agreement with the calculated Raman intensities². (These calculations took into account the non-linear dispersion of acoustic phonons in silver. As a result, the calculated vibration wavenumbers do not match.) As discussed before, (the $\text{SPH}, 2, 0$) mode is quite special even if we class it as a SPH_T mode. It changes the surface shape and therefore contributes significantly to inelastic light scattering. Other harmonics contribute significantly only when their URS is large and this in turn is very well correlated to their SPH_L nature as can be seen in Fig. 2.

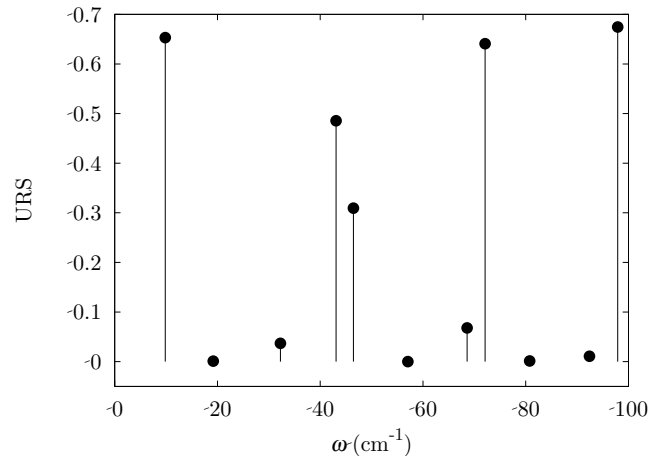


FIG. 5: Mean squared radial surface displacement (URS) as a function of wavenumber for $(\text{SPH}, \ell = 2)$ modes of a 5 nm diameter silver nanoparticle ($v_T/v_L = 0.464$).

Many experiments have observed peaks in Raman spectra attributed to acoustic phonon vibrations of silver^{6,7,8,9,10,11,12} silicon^{13,14} and $\text{CdS}_x\text{Se}_{1-x}$ ^{15,16,17,18,19}. These studies have regularly succeeded in observing the $(\text{SPH}, 2, 0)$ mode and the $(\text{SPH}, 0, 0)$ mode. A number of studies have seen $(\text{SPH}, 0, n)$ with n up to 4¹². However, there has never been a clear indication of Raman scattering from $(\text{SPH}, 2, 1)$ even though there have been determined efforts to see it.

At the same time, $(\text{SPH}_L, 2, n_L = 0)$ seems like a strong candidate to have noticeable Raman scattering, since it has strong radial surface motion as well as a strong u_L component that will give it stronger divergence in its interior.

It should be noted that $\ell = 0$ modes are always SPH_L . That is why no full circles are plotted in Fig. 3 on the T_{43} root curves at $\ell = 0$. This has been the source of many erroneous calculations in the past²⁰.

It is often claimed^{21,22,23,24} that modes with $n = 0$ are “surface modes” while modes with $n > 0$ are “inner modes”. The values of U2S in Tab. I show that this is a misconception. While this is true for $\ell = 0$ and 1, for $\ell = 2, 3$ and 4 it can be seen that $(\text{SPH}, \ell, 1)$ has the strongest surface motion relative to all (SPH, ℓ, n) .

Although Tab. I shows URS to be zero for $(\text{SPH}, 2, 1)$, the more precise value of v_T/v_L where URS is zero is 0.488. URS for $(\text{SPH}, 2, 1)$ is only near zero for v_T/v_L close to 0.488. However, URS remains small for $(\text{SPH}, 2, 1)$ for materials whose Poisson ratio is close to $\frac{1}{3}$.

which is true of many common materials. This contradicts a widespread misconception^{25,26,27} that SPH FSM modes always have a radial displacement component at the surface.

Acknowledgments

This work was supported by a Discovery Grant from the Natural Sciences and Engineering Research Council of Canada. L. M. L. Murray is thanked for suggestions. A. R. Laarakker is thanked for reading a draft manuscript.

* Electronic address: lucien.saviot@u-bourgogne.fr

† Electronic address: dbmurray@mail.silk.net

¹ H. Lamb, Proc. London Math. Soc. **13**, 189 (1882).

² G. Bachelier and A. Mlayah, Phys. Rev. B **69**, 205408 (2004).

³ A. C. Eringen and E. S. Suhubi, *Elastodynamics* (Academic, New York, 1975), vol. II, pp. 804–833.

⁴ D. B. Murray and L. Saviot, Phys. Rev. B **69**, 094305 (2004), cond-mat/0310099.

⁵ E. Duval, Phys. Rev. B **46**, 5795 (1992).

⁶ H. Portalès, L. Saviot, E. Duval, M. Fujii, S. Hayashi, N. Del Fatti, and F. Vallée, J. Chem. Phys. **115**, 3444 (2001).

⁷ H. Portalès, E., L. Saviot, M. Fujii, K. Sumitomo, and S. Hayashi, Phys. Rev. B **63**, 233402 (2001).

⁸ E. Duval, H. Portalès, L. Saviot, M. Fujii, K. Sumitomo, and S. Hayashi, Phys. Rev. B **63**, 075405 (2001).

⁹ M. Fujii, T. Nagareda, S. Hayashi, and K. Yamamoto, Phys. Rev. B **44**, 6243 (1991).

¹⁰ H. Portalès, Ph.D. thesis, Université Claude Bernard - Lyon I (2001).

¹¹ A. Courty, I. Lisiecki, and M. P. Pilani, J. Chem. Phys. **116**, 8074 (2002).

¹² A. Nelet, A. Crut, A. Arbouet, N. Del Fatti, F. Vallée, H. Portalès, L. Saviot, and E. Duval, Appl. Surf. Sci. **226**, 209 (2004).

¹³ M. Fujii, Y. Kanzawa, S. Hayashi, and K. Yamamoto, Phys. Rev. B **54**, 8373 (1996).

¹⁴ L. Saviot, D. B. Murray, and M. del C. Marco de Lucas, Phys. Rev. B **69**, 113402 (2004), cond-mat/0307634.

¹⁵ P. Verma, W. Cordts, G. Irmer, and J. Monecke, Phys. Rev. B **60**, 5778 (1999).

¹⁶ L. Saviot, B. Champagnon, E. Duval, I. A. Kudriavtsev, and A. I. Ekimov, J. Non-Cryst. Solids **197**, 238 (1996).

¹⁷ M. Ivanda, K. Babocs, C. Dem, M. Schmitt, M. Montagna, and W. Kiefer, Phys. Rev. B **67**, 235329 (2003).

¹⁸ G. Irmer, J. Monecke, P. Verma, G. Goerigk, and M. Herms, J. Appl. Phys. **88**, 1873 (2000).

¹⁹ L. Saviot, B. Champagnon, E. Duval, and A. I. Ekimov, Phys. Rev. B **57**, 341 (1998).

²⁰ L. Saviot, D. B. Murray, A. Mermet, and E. Duval, Phys. Rev. E **69**, 23901 (2004), cond-mat/0307112.

²¹ A. Tanaka, S. Onari, and T. Arai, Phys. Rev. B **47**, 1237 (1993).

²² A. Tamura, K. Higeta, and T. Ichinokawa, J. Phys. C: Solid State Phys. **15**, 4975 (1982).

²³ A. Tamura and T. Ichinokawa, J. Phys. C: Solid State Phys. **16**, 4779 (1983).

²⁴ N. N. Ovsyuk and V. N. Novikov, Phys. Rev. B **53**, 3113 (1996).

²⁵ I. Ohno, M. Abe, M. Kimura, Y. Hanayama, H. Oda, and I. Suzuki, American Mineralogist **85**, 288 (2000).

²⁶ C. Lomnitz and S. Nilsen-Hofseth, Eos **86**, 65 (2005).

²⁷ P. R. Heyliger and A. Jilani, Int. J. Solids Structures **29**, 2689 (1992).